

Experimental determination of the rate of flame spread across LNG pools

Graham Atkinson¹, Steven Betteridge², Jonathan Hall¹, James R. Hoyes¹ and Simon E. Gant¹

¹ Health and Safety Laboratory, Harpur Hill, Buxton, SK17 9JN.

² Shell Global Solutions (UK), Brabazon House, Concord Business Park, Threapwood Road, Manchester, M22 0RR.

In one of the very large LNG pool fire experiments conducted as part of the Phoenix tests for the US Department of Energy, the flames from the centrally-ignited pool fire did not cover the entire area of the LNG spill. This behaviour may be explained by the thermal updraft generated by the fire driving an inward flow of air and natural gas across the non-burning region that exceeded the burning velocity of the outwardly spreading flame front, thereby preventing the fire from spreading radially outwards to the extremities of the LNG spill.

This paper reports results from medium-scale experiments that have been carried out to test this hypothesis and hence quantify the maximum extent of a pool fire. The experiments were carried out using a 4 m long by 1 m wide LNG pool (50 mm deep) in a 1.2 m wide fire tunnel with controlled ventilation. The LNG vaporisation rate was controlled using an array of warm water sprays directed upwards onto the underside of the stainless steel LNG tray. In most of tests, the LNG vaporisation rate was $0.110 \text{ kg m}^{-2} \text{ s}^{-1}$ to simulate typical values for LNG pool fires on water. As expected, counter-flow flame spread was most rapid close to the walls of the tunnel where flow speeds were lowest and turbulence intensities were high. However, even close to the wall the backwards propagation of flame was prevented by an imposed velocity of 2.8 m s^{-1} or higher.

The experimental results support the hypothesis that a thermally-driven inflow can cause non-burning regions and that this is likely to have been the cause of the behaviour observed in the Phoenix tests. The critical velocity against which flames are unable to propagate is geometry dependent and the critical velocity in an open geometry is estimated to be 2 m s^{-1} . This result suggests that non-burning regions may be produced in centrally-ignited, unobstructed LNG spills with diameters of 20 m or more.

Keywords: LNG, pool fire, CFD, entrainment velocity.

Introduction

World production of liquefied natural gas (LNG) has increased from 160 mmtpa in 2007 to 246 mmtpa in 2014 (Wood Mackenzie, 2014). There have been corresponding increases in the number of facilities involved in the production and transportation of liquefied gas, including LNG tankers, LNG import and export facilities and proposed Floating LNG (FLNG) vessels that are currently being built. The increasing importance of LNG makes it more important to be able to assess the consequences of substantial losses of containment at all stages of the supply chain in order to manage the hazards appropriately.

One particular scenario is the potential spillage of large quantities of LNG into a harbour: the liquefied gas could spread out to form a large evaporating pool of LNG. If such a pool ignited there could be damaging levels of thermal radiation at large distances from the point of spillage. These could affect vessels and their crews as well as port facilities and on site populations. In addition to the immediate threat to the safety of those involved, there could be serious and long-lasting damage to public perception of the safety of LNG.

Assessment of the thermal radiation from such spill fires is not straightforward. There have been relatively few large-scale pool fire tests carried out on LNG and they have yielded some contradictory results. In a 35 m diameter bundled LNG pool fire test on land at Montoir (Nedelka *et al.*, 1990), the fire spread across the full area of the LNG spill and there was significant smoke production that reduced the effective surface emissive power (SEP) of the flame. On the other hand, in one of the Phoenix tests conducted by Sandia National Laboratory in 2009, the resultant pool fire from a nominal 80 m diameter LNG spill did not extend to the upwind edge of the LNG pool and produced relatively little smoke. The maximum extent of the burning area at the base of the flame in the test only corresponded to about 50% of the total area of the spill (Blanchat *et al.*, 2011). The flame height to fire diameter ratio was significantly higher than would have been expected from some established correlations (Thomas, 1963).

It has been suggested by Betteridge *et al.* (2014) that these variations in burning behaviour can be explained by the development of substantial non-burning regions around the periphery of very large LNG pool fires. High rates of vaporisation of LNG are sustained in these outer areas but the inwards flow across the surface (driven by convection in the central fire) is so strong that the flame cannot spread outwards across the whole pool spill. LNG vaporisation outside the burning area means that at low level the flames entrain a mixture of air and LNG rather than just air, which produces an increase in the total burning rate and flame height. The flame height to diameter ratio is greater than in fully burning pool fires because vaporisation occurs over a larger area than just the extent of the burning area.

Betteridge *et al.* (2014) estimated the strength of the inward flow across the surface of the non-burning areas of the LNG pool in the large Phoenix test by tracking the positions of visible turbulent eddies in video records. This analysis suggested a flow speed of 2 to 3 m s⁻¹.

Both Betteridge *et al.* (2014) and Kelsey *et al.* (2014) carried out computational fluid dynamics (CFD) modelling to investigate the flow close to the edge of a large LNG pool fire. Betteridge *et al.* (2014) used the ANSYS CFX code (ANSYS, 2012) where vaporisation in non-burning areas was included in the model and the fire was represented by a distributed heat source within a prescribed volume. The radial entrainment velocity at the edge of a 50 m diameter fire (in a 80 m diameter pool) was calculated to be 3.7 m s⁻¹.

Kelsey *et al.* (2014) used the Fire Dynamics Simulator (FDS) CFD code (McGrattan *et al.*, 2013) to investigate the sensitivity of the flow behaviour to assumptions about the burning rate, the radiative fraction, grid resolution and choice of turbulence model. The radial entrainment velocity predictions for pools of various sizes are shown in Table 1.

Table 1: Radial inflow velocity predictions from Kelsey *et al.* (2014). The range of values represents the variability due to the choice of turbulence model.

Fire diameter (m)	Burn rate 0.1 kg m ⁻² s ⁻¹	Burn rate 0.45 kg m ⁻² s ⁻¹
20	1.8 to 2.0 m s ⁻¹	2.0 to 2.2 m s ⁻¹
30	2.2 to 2.5 m s ⁻¹	2.6 m s ⁻¹
40	2.6 to 2.8 m s ⁻¹	3.0 m s ⁻¹
50	3.0 to 3.2 m s ⁻¹	3.4 m s ⁻¹

Note that a burn rate of 0.45 kg m⁻² s⁻¹ is substantially higher than established values (e.g. Luketa, 2011). It was used by Kelsey *et al.* (2014) to represent the increase in the total burning rate that may be associated with non-burning regions.

Flame speeds above liquid pools

For liquids at temperatures above their flashpoint, the rate of spread of fire is determined by propagation of a pre-mixed flame in the vapour above the surface. Experiments have been carried out with alcohols and jet fuels at temperatures up to about 50°C above their flashpoint (Gottuk and White, 2002). The maximum rate of flame spread was found to be approximately 2 m s⁻¹ and this velocity was not very sensitive to the temperature of the fluid above the flashpoint in the temperature range covered.

The above rate of flame spread is substantially greater than the laminar burning velocity for the materials concerned, which is 0.4–0.45 m s⁻¹ (Lewis and von Elbe, 1961). The reasons for this are two-fold:

- i. The laminar burning velocity is the rate at which the flame propagates into unburned gas in the frame in which the unburned gas is stationary. Generally, the unburned gas is moved by the expansion associated with combustion. For example, if the flame propagates away from the closed end of a tube, the unburned gas moves at a speed of $(\sigma-1)S_u$, where S_u is the burning velocity and σ is the expansion ratio during combustion. The observed flame speed in this case is σS_u . For flames in the open, like that above an LNG pool, the flame speed is expected to be $\sqrt{\sigma} S_u$ (Atkinson, 2012). This is roughly 2.5 S_u .
- ii. The flame front is generally curved (in the vertical plane) and this increases the perimeter over which the flame can progress into the unburned gas (Burgoyne and Roberts, 1968). This occurs even for laminar flames where the enhancement factor is about 1.5, but if the inflow to the flame is turbulent, the effective flame perimeter may be further extended. Only turbulence with a length scale comparable to, or somewhat smaller than, the depth of the flammable layer is effective in distorting the flame front and increasing the burning rate in this way.

The propagation of fire across the surface of liquids against an opposing air flow has also been studied for alcohols close to their flashpoint. Some typical results for methanol at 25°C (10°C above its flashpoint) are shown in Table 2 (Paxton and Dismile, 2013).

An opposing air flow of 2.6 m s⁻¹ does not halt the progress of the flame even though the flame speed in calm conditions is only 1.78 m s⁻¹ (see Table 2). For liquids that are within a few tens of degrees of their flashpoint, the flammable zone in which the flame propagates is very close to the liquid surface. Since the concentration at the liquid surface is within the

flammable range and any substantial dilution with air will take it outside the flammable range, it follows that the flow speed within the flammable layer is close to that of the liquid (i.e. zero) and consequently very much less than the speed of air outside the boundary layer.

Table 2: Flame spread velocities with and opposing an imposed airflow from Paxton and Dismile (2013)

Air speed (m s^{-1})	Flame velocity (m s^{-1})
- 2.6 (opposing flame spread)	+ 1.08
- 1.3 (opposing flame spread)	+ 1.65
0	+ 1.78
1.3 (with flame spread)	+ 1.76
2.6 (with flame spread)	+ 2.58

The situation for LNG spills on water is quite different. In this case the vapour within the boundary layer is too rich to support combustion. The mixture is only flammable in a thin layer well above the liquid surface where the flow speed is closer to that of the overlying airflow. In this case, one would expect flame spread to be prevented by an imposed airflow close to the speed of fire spread in the absence of any external flow. Consequently, non-burning areas are to be expected above LNG pools where the convective inflow exceeds the flame speed that occurs in the absence of external mean flow but with a comparable level of turbulence.

The primary objective of this study was to measure this turbulent flame speed and hence determine the critical airflow velocity that would prevent the spread of flame above an LNG pool. Most of the tests involved ignited LNG pools in which the flame spread against a controlled airflow. Two unignited tests were also carried out to measure the vaporisation rate associated with the ignited tests.

Experimental arrangement for ignited tests

The experiments were carried out in a specially constructed steel tunnel which was fitted with an array of fans at one end to allow a controlled flow of air to be provided. A shallow stainless steel tray in the middle part of the tunnel was half-filled with LNG to model a liquid spill. To drive the vaporisation of this LNG in a controllable way, jets of hot water were directed upwards onto the underside of the tray. The overall layout of the experiment is illustrated in Figure 1.

The overall depth of the LNG tray was 100 mm. Below the tray was a 200 mm deep skirt running around the perimeter. The purpose of this skirt was to provide additional stiffness and to support and enclose an array of 38 mm diameter (1.5") pipes that delivered the warm water spray through a set of 124 upward-facing 3 mm diameter holes. The flatness and levelness of the tray were monitored throughout the test series and even after a number of fire trials the tray remained flat and level to within approximately ± 2 mm.

A schematic showing the water system is shown in Figure 2. The hot water flow was driven by gravity with a head of 3 m. The hot water flow rate decreased during the experiment, due to lowering of the reservoir level, but the decrease in flow rate was limited to less than 5%. The flow rate was controlled by a single 51 mm diameter (2") valve which was remotely operated to be either shut or fully open. This gravity driven system provided a very reliable and reproducible flow of heat to the LNG tray. In Test 5, the water supply to alternate spray pipes was removed, which reduced the area directly exposed to heating jets and consequently reduced the vaporisation rate.

The air flow in the tunnel was driven by an array of fifteen 250 mm diameter fans (Type W2E250-H206-01 - manufactured by Ebm-papst). The velocity through the fan openings was relatively high ($\sim 15 \text{ m s}^{-1}$) and consequently the mixed flow in the tunnel was relatively insensitive to moderate external winds. The fan array is shown in Figure 3.

Velocity measurements in the tunnel were recorded using a TSI hotwire probe. The probe was located 1000 mm upstream of the LNG tray, in the centre of the tunnel width and at a height of 300 mm above the tunnel floor.

Flow straightening downstream of the fans was provided by a densely packed array of eighty 160 mm diameter, 1000 mm long rigid plastic pipes. The wall thickness of the pipes was 4 mm. When the flow straighteners were fitted, the maximum flow speed in the tunnel was 3.2 m s^{-1} . In one test, the air speed was reduced to approximately 2.8 m s^{-1} part way through the experiment. This involved switching off two of the fans (marked with yellow crosses in Figure 3).

Two tests were carried out at a lower speed (2.4 m s^{-1}). In this case a perforated plate (30% open area, hole diameter 3 mm) was used after the flow straightener to introduce additional back pressure in the inlet section.

The LNG was ignited using a gerb (a firework producing a shower of sparks), which was mounted in the ceiling. The edge of the zone affected by incendive sparks corresponded quite closely with the downstream edge of the LNG tray.

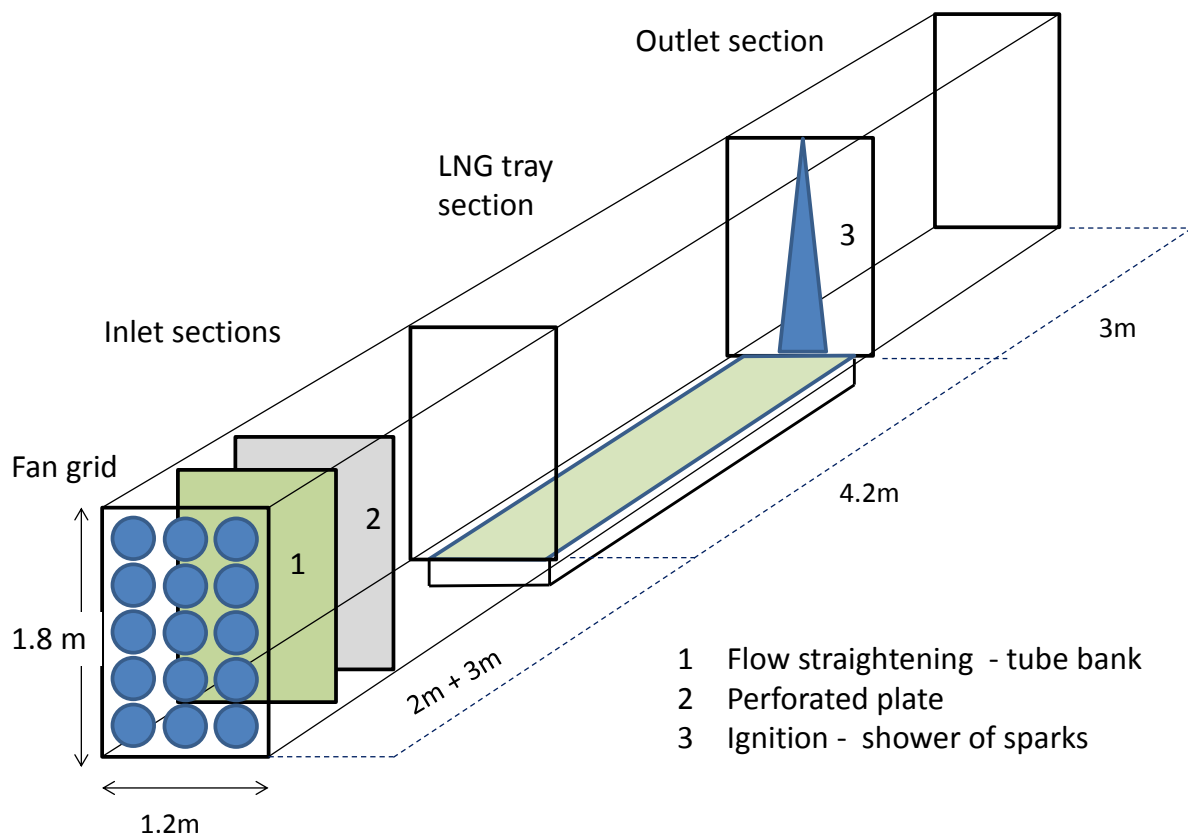


Figure 1: Schematic of the test rig for ignited tests

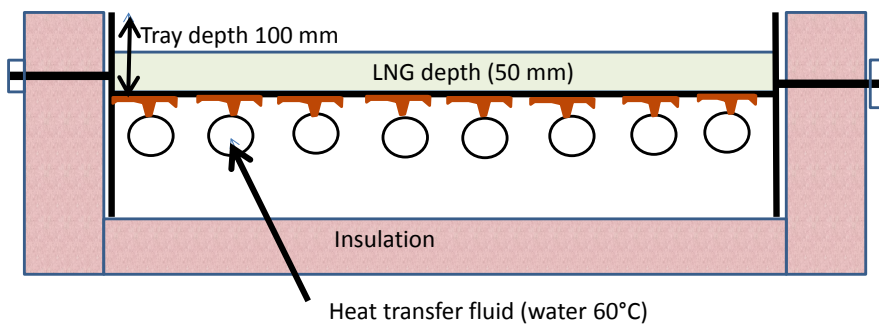


Figure 2: LNG tray and hot water system used to drive vaporisation



Figure 3: Fan array used to drive air through the tunnel

Experimental system for unignited tests

For the unignited test, a wooden extension (height 1000 mm, width 1200 mm and length 6000 mm) with a series of baffles was fitted to the end of the rig to mix the cold flow of unignited vapour (Figure 4). This subsequently restricted the maximum flow speed (in the main tunnel) to 1.9 m s^{-1} . An array of thermocouples at the outlet of the tunnel was used to monitor the completeness of mixing. Gas samples were taken from the mixed flow.



Figure 4: Mixed (unignited) vapour flow from the timber calibration tunnel (left) and low level unmixed gas current from the main tunnel prior to ignition in Test 2 (right)

Instrumentation for ignited tests

The ignited tests were instrumented with thermocouples to monitor:

- i. The development of the LNG pool during filling
- ii. The progress of flame across the pool surface
- iii. The delivered and waste water temperature

Progress of the flame was monitored by a number of CCTV cameras mounted in the tunnel ceiling.

Test programme

The conditions in the various tests are shown in Table 3. This table includes the ethane content of the two LNG deliveries used for the work. Levels of other gases within the LNG composition were negligible.

Table 3: Summary of test variables

Reference	Ignition	Airflow (m s ⁻¹)	Flow straighteners	Water temperature (°C)	Number of water jets	LNG tank fill (%)	Initial ethane fraction (mol%)
TEST 0	No	1.9	No	62	124	30	2.6
TEST 1	Yes	2.4	Yes	59	124	15	2.6
TEST 2	Yes	2.4	Yes	68	124	90	6.6
TEST 3	Yes	3.2	Yes	62	124	75	6.6
TEST 4	Yes	3.2 / 2.8	Yes	66	124	60	6.6
TEST 5	Yes	3.2	Yes	64	62	45	6.6
TEST 6	No	3.2	Yes	62	62	30	6.6

Summary of results

A basic summary of results from the tests is shown in Table 4. The test durations were estimated from the time that high vapour generation occurred (when the hot water jets were switched on) and up to the time when the thermocouples showed a large rise in temperature.

Table 4: Summary of test outcomes (*data unavailable)

Reference	Ignition	Airflow (m s ⁻¹)	Flame spread	Test duration t _{tot} (s)	Methane release duration t _{methane} (s)	Ethane release duration t _{ethane} (s)
TEST 0	No	1.9	N/A	145	103	42
TEST 1	Yes	2.4	Uncontrolled (RHS)	142	84	58
TEST 2	Yes	2.4	Uncontrolled (LHS/RHS)	130	97	33
TEST 3	Yes	3.2	Controlled	138	106	32
TEST 4	Yes	3.2 / 2.8	Controlled	*	105	*
TEST 5	Yes	3.2	Controlled	238	151	87
TEST 6	No	3.2	N/A	310	198	112

Discussion of experimental results

The data in Tables 3 and 4 show that for the high rate of water heating (Tests 0-4) the total duration of the test is not markedly changed by ignition. Since all of the tests were started with the same fill level, this finding confirms that in these tests the heat flux driving vaporisation comes mainly from the water spray under the metal tray, rather than convective or radiative heating by the flame. Consequently, the measurements of vaporisation rate in Test 0 provide a good guide to the rate of vaporisation during the ignited tests. Conversely, for the lower rate of heat release (Tests 5 and 6), the effect of heat transfer from flames significantly shortens the time required for complete vaporisation.

Figure 5 shows the typical variation in temperatures measured by thermocouples (TCs) situated 10 mm and 90 mm above the base of the tray. The plot has been annotated to show the various stages of the release. The start of very active methane vapour production is marked by a sharp drop in the temperature recorded by the 90 mm TC. Before the hot water jets are switched on, this TC is well above the liquid level but as the rate of bubble production increases the liquid swells up to engulf the device. This clearly marks the start of the main part of the release. As methane in the LNG pool starts to run out, the temperature of the liquid starts to rise ever more quickly: loss of methane is almost complete by the time the liquid temperature is a few tens of degrees above its boiling point. The temperature of the residue stabilises at the boiling point of ethane until this in turn has completely vaporised.

It is worth noting that the ethane content of the LNG is a function of the initial composition of the tank fill and of the storage tank level at the time of the test. Methane is preferentially lost by evaporation and so the relative concentration of ethane increases as the supply tank is emptied. Furthermore, methane is preferentially lost during the filling operation, which compounds the increase in ethane concentration. Measurements showed that approximately half of the methane delivered

was lost in the filling process and carried away in the airflow. Ethane losses during filling were not measured but are likely to be comparatively low.

The maximum methane vaporisation rate in the unignited case with a high level of heating was approximately $0.11 \text{ kg m}^{-2} \text{ s}^{-1}$, as shown in Figure 6. For the reduced heating setup (Tests 5 and 6) the rate of vaporisation was around $0.075 \text{ kg m}^{-2} \text{ s}^{-1}$.

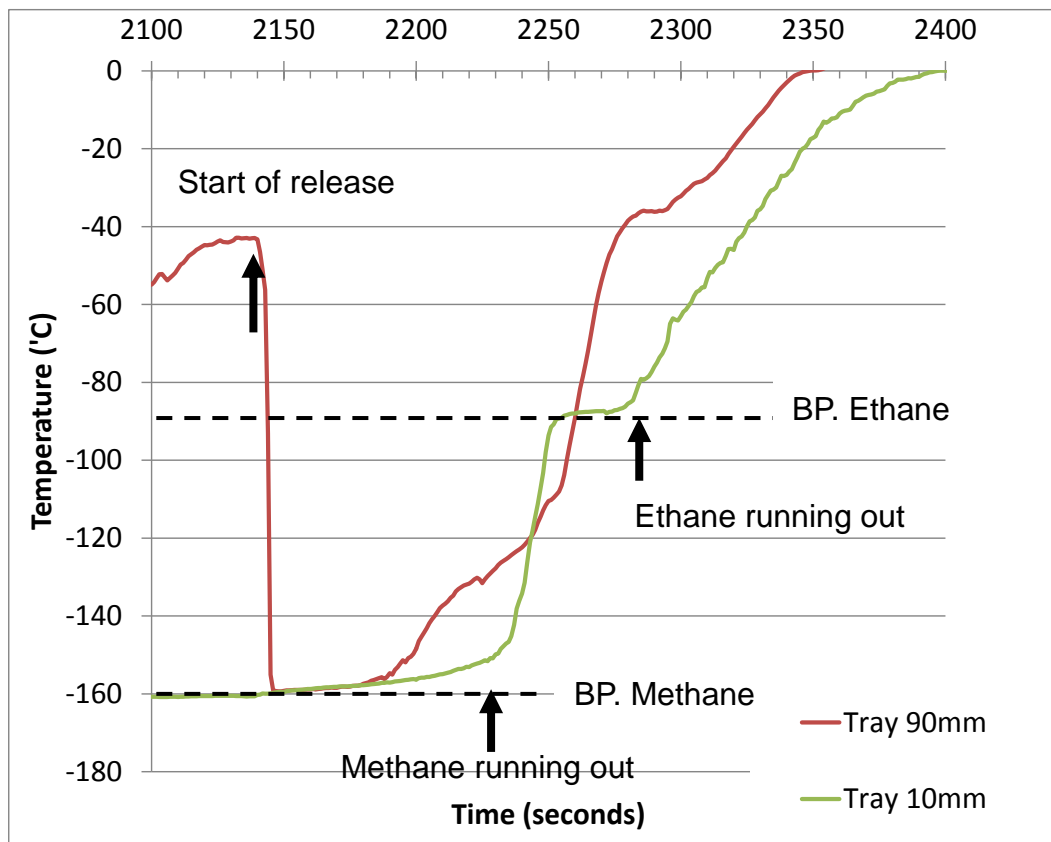


Figure 5: Thermocouple measurements during Test 0

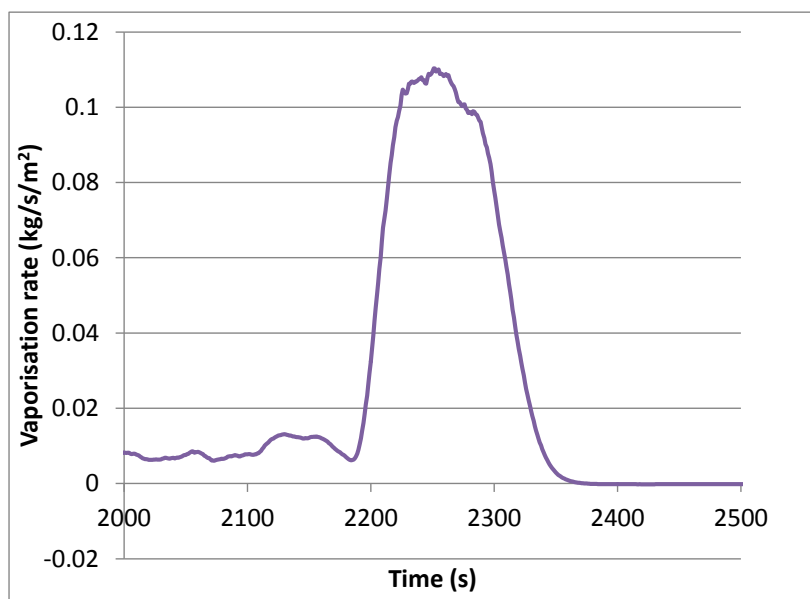


Figure 6: Methane vaporisation rate (for Tests 0-4) based on methane and velocity measurements from Test 0

Discussion of flame spread results

At an air flow of 2.4 m s^{-1} the flame spread back against the flow to the upwind edge of the tray (Tests 1 and 2). In these tests it was observed that the flame propagated in the low speed area close to the side walls and then spread sideways as it was convected downstream.

At air flows of 2.8 m s^{-1} and 3.2 m s^{-1} the progress of the flame in an upstream direction was arrested part way down the tunnel. Again the spread of flame was most rapid in the low speed flow close to the walls, but the imposed airflow was sufficient to prevent sustained flame spread even in these regions. Consequently, the resultant quasi-steady flame fronts on both sides of the tunnel form a characteristic V-shape when viewed from above, as can be seen in Figure 7. In this image, well-mixed regions burn with a blue flame and are orientated at an angle, θ , with the incident air flow. The component of the air speed perpendicular to the flame front can therefore be calculated and used as a basis for estimating the turbulent flame speed relative to gas with zero average velocity.

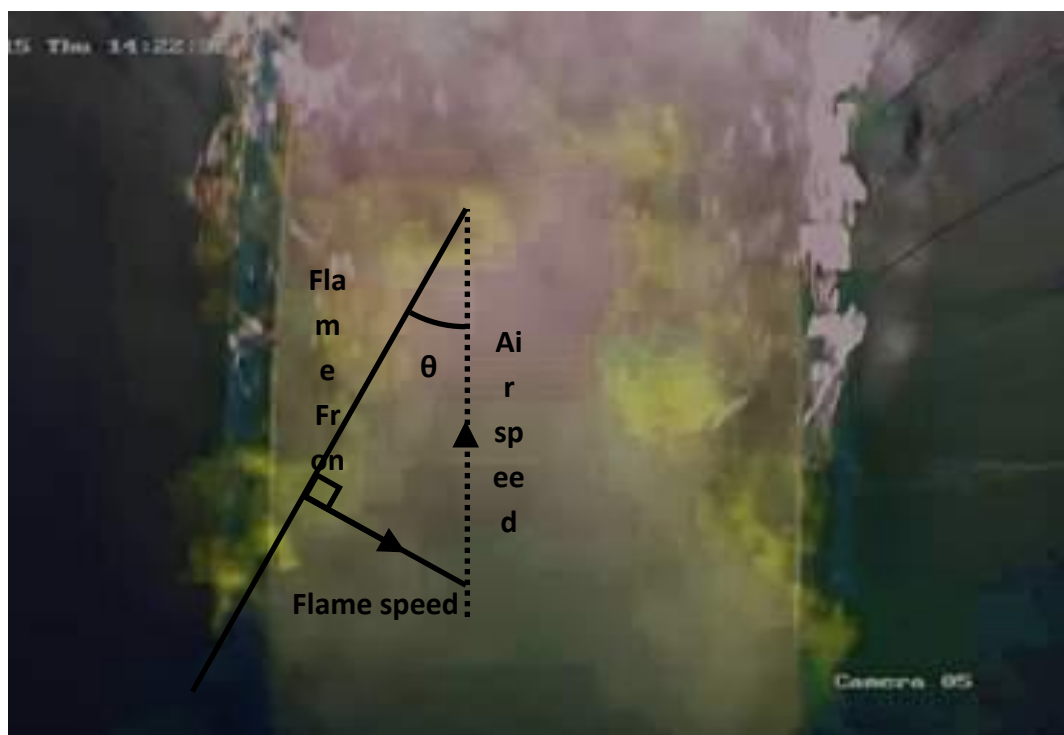


Figure 7: Angle between flame front and air speed. The image above is the original image, which has been colourised and annotated below

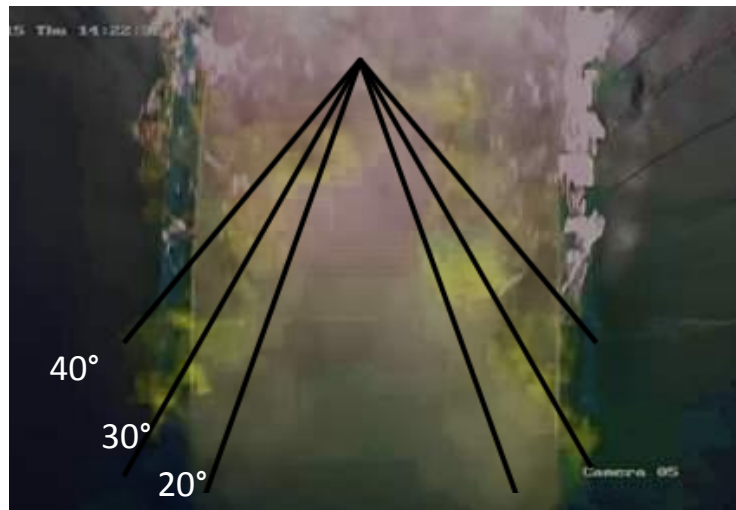


Figure 8: Image of flame superimposed on lines indicating 20° , 30° and 40° inclination to the free stream

Analysis of the video footage recorded during Tests 3 and 4, during the time period when the air flow arrested the flame spread, showed that the angle, θ , varied between 20° and 40° (Figure 7 and Figure 8). The resultant calculations, shown in Table 5, suggest a maximum turbulent flame speed of about 2.0 m s^{-1} , which is broadly in line with other experiments on flame spread over liquid pools (Burgoyne and Roberts, 1968; Gottuk and White, 2002). This value also agrees well with the measured rate of spread of flame in methane layers, where the methane concentration was close to 100% at the roof of a mine gallery and declined with depth through the layer. In this case, the measured flame speed was 1.8 m s^{-1} and it showed little sensitivity to the overall depth of the methane layer or thickness of the flammable zone (Phillips, 1965).

Table 5: Flame speeds estimated from flame angles for air flows of 2.8 m s^{-1} and 3.2 m s^{-1}

θ (deg)	$\sin(\theta)$	Turbulent flame speed (m s^{-1})	
		For $u_{air} = 2.8\text{ m s}^{-1}$	For $u_{air} = 3.2\text{ m s}^{-1}$
20	0.34	1.0	1.1
30	0.50	1.4	1.6
40	0.64	1.8	2.0

Implications for spread of flame across LNG pools

The discussion in the introduction concluded that the flame velocity in the flammable zone is close to that in the free-stream for LNG spills on water and that the rate of turbulent flame spread would equal the air velocity necessary to hold back flame spread. It follows that flame spread across the surface of an LNG pool is likely to be held back where there is an opposing flow across the pool of more than 2.0 m s^{-1} .

Modelling of radial inflow by Kelsey *et al.* (2014) using FDS (see Table 1) suggests that inflow speeds will exceed 2.0 m s^{-1} if the pool diameter is greater than about 20 m. These predictions are largely independent of the vaporisation rate in the range 0.1 to $0.45\text{ kg m}^{-2}\text{ s}^{-1}$ and they suggest that in completely unobstructed pools, the maximum diameter of burning areas would be of the order of 20 m.

Flame spread across the LNG pool surface will be promoted by solid obstructions and external winds. For example, the flame in the Phoenix test was affected by a cross-wind of around 1.6 m s^{-1} and the loading boom running to the centre of the pool roughly perpendicular to the wind. The result was a flame that was anchored by the boom, extending a short distance upwind and extensively downwind. Consequently, the maximum overall fire diameter was around 50 m, rather than the smaller 20 m predicted in an unobstructed pool. In the Montoir tests, flames would have been stabilised by the rim of the bunded pool, again allowing more extensive flame spread than might have been observed in a spill on open water without solid obstructions (and associated wake areas) around the edge.

Potential effects of changes in scale, turbulence and radiation

This section considers how the propagation of a flame in the experiments would be affected by turbulence in the flow and how this might vary in larger pools.

Observation of the flow show that the length scale of the largest eddies is similar to the total depth of the mixing layer which was 100- 400 mm in these experiments. Analysis of the development of large eddies visible in videos of the unburned flow suggests a turbulent velocity (at this large scale) of around 0.1 m s^{-1} .

These eddies move the flame around (and after ignition are responsible for the variations in the flame front angle obvious in Figure 7), but they do not increase the rate at which the flame progresses into the unburned gas. This is because they are associated with curvatures in streamline that are too large to deform the flame front. Previous CFD analysis (Betteridge *et al.*, 2014) suggests that the flame is confined to a thin layer corresponding to about 10% of the total thickness of the mixing layer. Consequently only turbulent eddies of the order of 10 - 40 mm in size would directly enhance the burning rate. The turbulent velocity associated with these smaller eddies would be about 30% of the velocity associated with primary eddies i.e. 0.03 m/s .

For large-scale, low-intensity turbulence, the interaction between a wrinkled flame front and the turbulent flow field is a largely kinematic effect and independent of length scale. There a number of correlations for turbulent burning velocity with turbulent velocity Poinsot and Veynante (2005) and Damkoehler (1947). These correlations suggest the turbulent burning velocity in the experimental case would be 5 - 10 % above the laminar value, with corresponding proportional increases in turbulent flame speed over the laminar flame speed. It is unlikely that the importance of turbulence will increase significantly for the changes in Reynolds number between the experiment and full scale for *equivalent geometries*.

However, the potential for flame spread against a convectively driven radial inflow could be significantly increased by congestion elements in the non-burning areas with a length scale comparable to the depth of the flammable layer. At full scale this would correspond to obstacles a few hundred millimetres in diameter within a few metres of the water surface. In the context of a spill on open water, such obstacles are unlikely to be found in practice.

A comparison between the current measurements of flame speed and other work on smaller scale (laminar) methane flames in mixing layers also needs to account for the temperature of the mixture. The temperature of the gas when the mixture was stoichiometric is estimated to have been -5°C . The temperature variation of laminar flame speed can be estimated from correlations given by Poinsot and Veynante (2005); at -5°C the laminar flame speed would be approximately 10% less than in the tests reported by Phillips (1965). It is therefore likely, in comparison with the work of Phillips, that the small effect on burning rate of increased turbulence in the current tests was largely off-set by the reduced temperature of the mixture. Our measurements of flame speed in an open mixing layer are in fact broadly in line with the value of 1.8 m s^{-1} reported by Phillips. As previously noted these figures for flame speed are much greater than the burning velocity because of the expansion associated with combustion and curvature of the flame front.

Conclusions

In a series of medium-scale experiments conducted at HSL, the rate of turbulent flame spread over the surface of a 4 m LNG pool was observed to vary between 1.0 and 2.0 m s^{-1} , which is low compared with the inflow velocity that would be driven by a large LNG pool fire. This observation supports the hypothesis of Betteridge *et al.* (2014) that substantial non-burning areas observed in the Phoenix LNG test were caused by the flame being unable to spread upwind against the convective-driven flow generated by the fire.

It is argued that the effect of turbulence on flame spread is relatively minor in the experimental case and that this would also be the case for larger pools, so long as the flow across the surface is not disturbed by solid obstacles.

The work suggests that flame spread over an LNG spill on open water would be arrested when the fire-driven inflow reached a level of 2.0 m s^{-1} or less. Previous CFD analysis (Kelsey *et al.*, 2014) suggests that this corresponds to a fire diameter of approximately 20 m.

The wind speed may be significantly higher than 2.0 m s^{-1} in real scenarios. Consequently, it is hypothesised that any flames will be blown downwind, resulting in a pool fire, with a diameter up to 20 m, moving towards the downwind edge of the spill area.

Larger diameter pool fires can be achieved if the flames are stabilised by solid obstacles at the water surface, which create wake areas that are sheltered from the convection driven flow. This effect explains why a larger burning area of around 50 m in diameter was observed during the large-scale Phoenix test, which was affected by a cross-wind of around 1.6 m s^{-1} and the presence of a loading boom running to the centre of the pool.

The experiments and analysis in this paper and the previous papers (Betteridge *et al* 2014, Kelsey *et al* 2014) show that it is overly simplistic to assume that a fire will cover the full surface of an unobstructed LNG spill, irrespective of the spill area. Instead, for large spills, the work indicates that a fire will only spread across a proportion of the spill surface and be located towards the downwind edge of the spill. Consequently, thermal radiation from the pool fire will be lower on the upwind side of the spill and higher on the downwind side than is currently predicted; which is likely to affect consequence assessments for LNG spills in harbours and/or ship transfers. Further work should consider how the prevailing wind, ignition location, sea state and the potential for the flame to anchor to structures may influence the pool fire size and subsequent thermal radiation consequences.

Acknowledgement

The work described in this paper was undertaken by the Health and Safety Laboratory (HSL) under contract to Shell Research Ltd, as part of a portfolio of process safety research projects sponsored by the Shell LNG Technology Platform.

References

- ANSYS, 2012, ANSYS CFX-Solver Modeling Guide. ANSYS, Inc., Canonsburg, Pennsylvania, USA. Release 14.5, October 2012.
- Atkinson, G.T., 2012, Effects of constraints on gas flow on the severity of vapour cloud explosions, IChemE Hazards 23 Conference, Symposium Series No. 158. (Available from: https://www.icheme.org/~media/Documents/Subject%20Groups/Safety_Loss_Prevention/Hazards%20Archive/XXIII/XXII_I-Paper-59.pdf, accessed 14 October 2015).
- Betteridge, S., Hoyes, J.R., Gant, S.E. and Ivings, M.J., 2014, Consequence modelling of large LNG pool fires on water, IChemE Hazards 24 Conference, Edinburgh, UK, May 2014.
- Blanchat, T., Helmick, P., Jensen, R., Luket,a A., Deola, R., Suo-Anttila, S., Mercie,r J., Miller, T., Ricks, A., Simpson, R., Demosthenous, B., Tieszen, S., and Hightower, M., 2011, The Phoenix series large scale LNG pool fire experiments, SAND2010-8676, Sandia National Laboratories, Albuquerque, NM.
- Burgoyne, J.H. and Roberts, A.F., 1968, The spread of flame across a liquid surface, Proc. Roy. Soc. A. 308: 55-68.
- Damkoehler, G., 1947, The Effect of Turbulence on the Flame Velocity in Gas Mixtures, Zeitschrift fuer Elektrochemie und Angewandte Physikalische Chemie, 46(11): 601-626 also (in English) NACA-TM-1112.
- Gottuk, D.T. and White, D.A., 2002, Liquid Fuel Fires. Chapter 15, Section 2, SFPE Handbook of Fire Protection Engineering, 3rd Edition. National Fire Protection Association, Inc., Quincy, Massachusetts, USA.
- Kelsey, A., Gant, S.E., McNally, K. and Betteridge, S., 2014, Application of global sensitivity analysis to FDS simulations of large LNG fire plumes, IChemE Hazards 24 Conference, Edinburgh, UK, May 2014. (Available from: https://www.icheme.org/~media/Documents/Subject%20Groups/Safety_Loss_Prevention/Hazards%20Archive/XXIV/XXI_V-Paper-33.pdf, accessed 24 December 2015).
- Lewis, B., and von Elbe, G., 1961, Combustion, flames and explosions of gases, Second Edition. Academic Press, New York.
- Luketa, A. (2011). Recommendations on the Prediction of Thermal Hazard Distances from Large Liquefied Natural Gas Pool Fires on Water for Solid Flame Models. Sandia National Laboratories report, SAND2011-9415, December 2011.
- McGrattan, K., Hostikka, S., McDermott, R., Floyd, J., Weinschenk, C. and Overholt, K., 2013, Fire Dynamics Simulator Technical Reference Guide Volume 1: Mathematical Model, NIST Special Publication 1018, Sixth Edition.
- Nedelka, D., Moorhouse J., and Tucker, R.F., 1990, The Montoir 35m diameter LNG pool fire experiments, Proc. 9th Int. conf. on LNG, Nice, 17-20 Oct, 1989, Publ. Institute of Gas Technology, Chicago.
- Paxton, B and Dismile, P., 2013, Flame spread over liquid pools, Aviation Fire Dynamics presentation, University of Cincinnati, USA. (Available from: http://www.ase.uc.edu/~pdisimil/classnotes/Aviation%20Fire%20Dynamics/Reserach%20Papers/FlameSpread_Paxton_05A_pr2013.pptx, accessed 24 December 2015).
- Phillips, H., 1965, Flame in a buoyant methane layer, 10th Int.Symp. on Combustion, The Combustion Institute, p.1277.
- Poinsot, T. and Veynante, D., 2005, Theoretical and Numerical Combustion, Pub. R.T. Edwards Inc.
- Thomas, P.H., 1963, The size of fires from natural fires, Proc. 9th Int. Symp. on Combustion, The Combustion Institute.
- Wood Mackenzie, 2014, Global LNG Industry Review. (Available from: <http://www.woodmac.com>, accessed 24 December 2015).